International Journal of Mass Spectrometry 325–327 (2012) 139–149

Contents lists available at SciVerse ScienceDirect

International Journal of Mass Spectrometry

journal homepage: www.elsevier.com/locate/ijms

The influence glutamic acid in protonated $b_3 \rightarrow b_2$ formation from VGEIG and related analogs

Lindsay Morrison, Árpád Somogyi, Vicki H. Wysocki*

Department of Chemistry and Biochemistry, University of Arizona, Tucson, AZ, United States

ARTICLE INFO

Article history:
Received 22 May 2012
Received in revised form 7 August 2012
Accepted 7 August 2012
Available online 17 August 2012

Keywords:
Alpha proton scrambling
b_3 ion
Anhydride
Peptide fragmentation

ABSTRACT

A direct pathway for the fragmentation of peptide b_3 fragment ions to b_2 ions has, until now, not been identified. Experimental evidence for the formation of a b_3 anhydride structure and isomerization to an extended macrocycle is demonstrated here by comparison of the completely different fragmentation patterns of the b_3 ions generated from protonated VGEIG and its methyl ester. In particular, the absence of a b_2 ion in the fragmentation spectrum of the methyl ester b_3 indicates that facile fragmentation of an anhydride-type b_3 is responsible for virtually all b_2 ions formed. The stability of this b_3 structure and the ease with which it fragments to the b_2 may be responsible for the relatively high abundance of the b_3 and b_2 ions. IRMPD action spectroscopy measurements indicate the presence of a ring protonated oxazolone in the b_2 population. VGEIG and three related analogs, VA_LEIG, VA_DEIG, and V(Aib)EIG were studied by QCID-HDX-SORI experiments in an FT-ICR instrument, and provide significant evidence for extensive alpha proton scrambling in an ion–molecule complex formed between the b_2 and neutral loss fragment following formation of the b_2. MS^3 and HDX of VG(2,2-d2)EIG indicate that the scrambled b_2 ions have the same structure as the unscrambled b_2. Based on these data and with the support of molecular modeling, we propose a new mechanism for this scrambling, in which the alpha protons are transferred in a multi-step pathway during an ion–molecule complex formed between the b_2 and amino-terminated anhydride ring neutral loss component.

1. Introduction

Mass spectrometry and tandem mass spectrometry have played an integral role in peptide sequencing in the field of proteomics for many years. By using low energy collision induced dissociation (eV CID), both singly and multiply charged peptides are activated and subsequent, charged directed fragmentation occurs at the most labile bonds. In peptides, these are typically the backbone amide bonds, the cleavage of which generates b and y type ions, as defined by the Roepstorff/Biemann nomenclature [1,2]. To date, a number of algorithms, such as SEQUEST, Mascot, and OMSSA compare and score experimental tandem mass spectra against theoretical spectra generated from a database of candidate sequences; thus, sequencing peptides from protein digests has become relatively common [3–5]. However, the identity of the amino acids on either side of the peptide bond, the length of the peptide, the number of charges, and the presence of acidic and basic sites on the peptide have been shown to play a role in the preference for fragmentation at particular peptide bonds [6–9]. Because of this, fragmentation efficiency at individual peptide bonds is not equal, and suppressed or enhanced cleavages often disrupt the sequencing of unknown peptides. As a result, many spectra remain unassigned or are incorrectly assigned [8–11]. In order to make sequence prediction more reliable, work has been done both to improve algorithm scoring models and to better understand the specific processes that dictate peptide fragmentation. The incorporation of peak intensity into scoring algorithms has become a poignant goal recently, as it is believed that a more finely tuned scoring model will lead to improved rates of identification. Indeed, a recent algorithm, SQID, has demonstrated the promise of this strategy with the incorporation of coarse intensity prediction into the scoring scheme [12]. An intensity based strategy for peptide identification, however, benefits from a more thorough understanding of the structural and sequence based motifs that lead to enhanced and suppressed cleavages at particular residues in order to predict spectra accurately. Experimentally, instruments with ultrahigh resolution and mass accuracy (<1 ppm error), such as LTQ-Orbitrap or Fourier transform ion cyclotron resonance (FT-ICR) instruments are more generally used to improve precursor and fragment ion assignments. The FT-ICR and ion trap instruments can be "coupled" with gas-phase deuterium exchange and IRMPD action spectroscopy [13,14]. These techniques, together with ion mobility, provide further insight and

* Corresponding author.
E-mail address: vwysocki@email.arizona.edu (V.H. Wysocki).

1387-3806/$ – see front matter © 2012 Elsevier B.V. All rights reserved.
http://dx.doi.org/10.1016/j.ijms.2012.08.012

details of isomeric ion structures that may be related to different pathways of protonated peptide fragmentation [15].

Several models have been developed to explain trends in fragmentation behavior, including the mobile proton model [16] and the pathways in competition model [17]. A detailed review of these models and other aspects of peptide fragmentation mechanisms has been published [17]. In the mobile proton model, the presence or absence of a mobile proton changes both the threshold for bond dissociation and the frequency of enhanced cleavage at acidic residues; this is largely due to the activation of charge-directed fragmentation pathways in the presence of a mobile proton [8,16]. The pathways in competition (PIC) model, which largely encompasses the mobile proton model, views an individual fragmentation as a series of pre-dissociation, dissociation, and post-dissociation events [17]. A deeper understanding of each of these events and the contributing factors in each stage, such as the proton affinity of fragments and the kinetics of individual pathways, is sought in order to better predict and explain peptide fragmentation at a mechanistic level [18].

Enhanced cleavage at acidic residues has been demonstrated for many years; however, this effect has primarily been demonstrated in peptides lacking a mobile proton. Systems with a fixed charge or metal adduct experience cleavage exclusively C-terminal to the acidic residue [19–25]. Presumably, the acidic proton bridges to the amide group at the acidic residue, activating the amide bond and permitting formation of a five-membered anhydride ring b ion and neutral y fragment [16,20]. In addition, Van Stipdonk and co-workers have shown enhanced cleavage C-terminal of aspartic acid in the fragmentation of YADFLG, in which the charging proton can be mobile, but detected no enhanced cleavage in the fragmentation of YAEFLG [6]. Other studies have shown small enhancements in fragmentation at the C-terminus of glutamic acid, but a definitive trend for C-terminal cleavage has not been established [8,21,26,27]. Wysocki and co-workers employed a data mining approach to characterize a set of doubly charged tryptic peptides. It was found that while glutamic acid and aspartic acid featured in peptides with roughly equal frequency, the extent to which the residue impacted local fragmentation was measurably different for the two. This differential behavior in enhanced cleavage between glutamic acid and aspartic acid containing peptides is well known and thought to be related to ring size of reaction intermediates or transition states, however is nonetheless incompletely understood, as a clear picture of how glutamic acid impacts fragmentation has yet to be established [22,28].

In this study we use tandem mass spectrometry, MS^3, variable wavelength IRMPD action spectroscopy [14], gas-phase hydrogen/deuterium exchange (HDX) [13], double resonance [29], and computational modeling to elucidate the structures and fragmentation pathways of a protonated model peptide VGEIG. The aliphatic residues of variable identity eliminate the possibility that fragments formed via cyclization will overlap with standard b ions. Placing unreactive functional groups at these residues additionally simplifies the fragmentation at other residues and prevents unusual fragmentation chemistries that may result from sidechain–sidechain interactions. In particular, the fragments formed by cleavage C-terminal and N-terminal to the acidic residue (b_3 and b_2 respectively) are examined along with the pathway by which b_3 fragments to b_2.

2. Materials and methods

2.1. Peptide synthesis and chemical modifications

Standard FMOC-protected amino acids and Wang resin were obtained from Novabiochem (San Diego, CA), FMOC-L-α-tert-butyl-glutamic acid was obtained from Chem-Impex (Wood-Dale, Il). Glycine-2,2-d2 was obtained from Sigma–Aldrich (St. Louis, Mo) and FMOC protected by a standard protection protocol [30]. Peptides were synthesized in house using standard FMOC solid phase peptide synthesis chemistry as described previously [31]. Briefly, N-terminally FMOC protected amino acids were stepwise added to Wang resin using O-benzotriazole-N,N,N′,N′-tetramethyl-uronium-hexafluoro-phosphate (HBtU) and N,N-diisopropylethylamine (DIEA) to promote formation of the amide bond. 70:30 DMF:piperidine was used to deprotect the N-terminus of the peptide prior to coupling. The peptide was cleaved from the polystyrene bead by incubation in 95% trifluoroacetic acid (TFA). Peptides were twice extracted in diethyl ether and diluted into 1:1:0.1% acetonitrile/H_2O/formic acid electrospray solvent before characterization by mass spectrometry.

O-methylation of carboxylic acid functionalities was achieved by adding 30 μL of 1 M acetyl chloride in anhydrous methanol to 100 mg of resin-cleaved and deprotected peptide. The reaction was quenched by dilution into the ESI spray solvent.

2.2. Mass spectrometry

A Bruker Daltronics 9.4 T FT-ICR was used for quadrupole CID (QCID) and sustained off-resonance irradiation (SORI) studies. Peptides were introduced by electrospray ionization (ESI) using an Apollo II ESI source with a flow rate of 160 μL/h. Quadrupole CID was performed by monoisotopic isolation of singly charged precursor ions by quadrupole isolation before activation by collision induced dissociation (CID) in the collision cell using Ar gas and (laboratory) collision energies that were varied from 1 to 21 eV. Fragment ions were transmitted into the ICR cell for detection or further activation by SORI. In particular, MS^3 was performed by monoisopically isolating b_3 ions generated by quadrupole CID by sweeping a notched frequency pulse across the appropriate frequency domain inside the ICR cell and simultaneously pulsing Ar gas into the cell. The b_3 ions were subsequently activated by SORI irradiation for 100 ms with a 600 Hz off-resonance pulse. The intensity of the off-resonance waveform is expressed as a percentage of the maximum wave amplitude; 1.2% was used in all experiments. The addition of an external, secondary waveform during the SORI pulse allowed for the complete ejection of ions at a particular m/z, that is, double resonance. The maximum amplitude of the square pulse overlapped temporally with the SORI excitation pulse such that ejection of the double resonance ion was achieved as rapidly as possible.

QCID-HDX-SORI experiments were performed using quadrupole isolation to monoisotopically isolate and fragment the precursor before transmitting the precursor and fragment ions to the ICR cell for hydrogen/deuterium exchange (HDX) and MS^3. CD_3OD was introduced to the ICR cell via an external leak valve system and permitted to exchange with fragment ions for 20 s. The external pressure of CD_3OD before introduction to the mass spectrometer was 8.1 mbar and the typical pressure within the ICR cell during exchange was 1×10^{-7} mbar. CD_3OD was removed from the ICR cell during a 60 s pumpdown interval before subsequent activation of the deuterated b_3 by SORI, performed as described above.

IRMPD action spectra were recorded at the CLIO Free Electron Laser Facility (Orsay, France) as described previously [32]. Briefly, a free electron laser was used to fragment b_3 and b_2 ions across the IR frequency range of 1000–2000 cm^{-1}. The fragmentation efficiency to produce individual or all observed ions from precursor was then plotted against the IR frequency (wavenumbers, cm^{-1}) to generate the variable wavelength IRMPD dissociation spectra.

2.3. Computational modeling

Theoretical structures were identified by first generating a collection of reasonable computational structures using a Monte Carlo simulation [33]. Four structures, a C-terminal oxazolone, macrocycle tripeptide, anhydride, and extended macrocycle tripeptide, formed by attack of the amino terminus on the third amide carbonyl, were each considered, and a collection of conformations was generated for the basic sites of each structure. Amide nitrogen protonation sites were not considered due to their low basicity. The prospective conformations were subsequently optimized at increasingly complex basis sets and conformers with redundant bridging were excluded at each level only if there existed an isomer with identical bridging at least 12 kcal/mol lower in energy. Final optimizations and frequency calculations were performed at the B3LYP 6-311++G** level of optimization and computed frequency spectra were scaled uniformly with a 0.978 scaling factor.

3. Results and discussion

3.1. QCID and double resonance

Fig. 1a shows the 12 eV QCID MS/MS spectrum of protonated VGEIG. Intense fragment peaks are detected at m/z 399 (b_4), 271 (a_4), and 286 (b_3) when relatively low collision energies (0–14 eV) are applied. At higher energies (>14 eV), the b_2 (m/z 157) becomes the second most dominant peak in the spectrum, second only to the b_3. Fig. 1b shows the energy resolved mass spectral plot that demonstrates this energy dependence in b_2 ion intensity. An interesting feature of this plot is the relatively high onset energy of the b_2 ion; at 9 eV, its appearance coincides not with the disappearance of the parent but rather the disappearance of the b_3 ion, suggesting that the b_3 ion is a major intermediate in b_2 formation. This is particularly useful as the b_3 structure associated with cleavage C-terminal to the acidic residue can be studied in order to better understand the factors that contribute to the intensity of the b_2 peak. The b_3 and a_4 ions appear to have the same onset energy of approximately 2 eV and the a_4 could, in principle, directly fragment to b_2. Double resonance studies were performed to eliminate the b_3 ion in order to verify that the a_4 does not directly fragment to b_2 and the results are shown in Fig. 1c and d. MS^3 fragmentation of the MH was performed with continuous ejection of ions in the range m/z 284–288 (m/z of the b_3 is 286.14). As the amplitude of the double resonance waveform is systematically increased, a larger fraction of the b_3 is removed from the ICR cell as is seen by the decrease in the b_3/MH ratio. In conjunction with this, the ratio of b_2/MH likewise decreases with increasing double resonance power, such that at the maximum double resonance amplitude neither ion species is resolvable from the noise, as shown in Fig. 1c. Double resonance and energy resolved mass spectrometry demonstrate that the formation of b_2 from any precursor requires a b_3 intermediate.

Although a direct fragmentation pathway between the b_3 and b_2 ions has not been demonstrated, the a_3 has been shown in some cases, wherein the b_3 is presumably an oxazolone structure, to be an intermediate along this pathway [34,35]. However, in the VGEIG system, the a_3 ion has an onset energy of 12 eV and a maximum relative abundance of less than 5%; as the b_2 has an onset energy 3 eV lower (9 eV), this suggests that the a_3 plays a minor, if any, role in the fragmentation pathway of $b_3 \rightarrow b_2$. Formation of the b_2 ion is thus almost entirely dependent on a b_3 intermediate, the structure of which must be understood in order to understand the fragmentation intensities of downstream ions such as the b_2.

MS^3 of the b_3 ion generated from protonated VGEIG is shown in Fig. 2a. The most striking features of this spectrum are the intense b_2 ion (m/z 157), the internal GE ion (m/z 187), and the ion at m/z 130.05, the charged complementary fragment to the b_2. (Note that all precursor and fragment ion masses were measured with high mass accuracy (with <2 ppm error) so the chemical compositions and assignments are fully justified.) The internal GE fragment can conceivably form by two pathways: fragmentation of the VG peptide bond, resulting in the formation of a b_1 acylium or GE ion, and by cyclization of the b_3, resulting in the formation of a macrocycle which can open at a different residue and fragment via the pathways of a permutated b_3 ion. Yalcin et al. have shown that b ions fragment with large kinetic energy releases, from which it was established that the acylium structure is not probable [36]. Spectroscopic studies have additionally confirmed that the oxazolone is the dominant b ion structure [37]. Formation of the GE ion is therefore more likely the result of cyclization via nucleophilic attack of the N-terminus on the glutamic acid carbonyl carbon [38]. Using a combination of hydrogen/deuterium exchange and IRMPD spectroscopy experiments on leucine-enkephalin and oligioglycine, Polfer and co-workers have shown the abundance of the b_3 macrocycle is very low: 6% in leucine-enkephalin and 0% in octaglycine, presumably because this pathway is kinetically or thermodynamically unfavorable [39]. From the VGE macrocycle, formation of a ring opened GEV could produce a GE b2 ion equivalent, in which cleavage of the VG bond would be favored by enhanced cleavage C-terminal to V and N-terminal to G.

In order to determine the extent to which the glutamic acid side chain is involved in macrocycle formation, a series of permuted VGE analogs were studied by MS^3. Fragmentation of the b_3 from protonated peptides GEVIG and EVGIG shows no evidence for the formation of a 9-membered b_3 macrocycle (Supplementary Information, Fig. 1), as internal (not "conventional" N-terminal type) b_2 ions for these peptides do not form. Alternatively, the b_3 of protonated G-γ-EVIG and γ-EVGIG demonstrate near identical fragmentation behavior when MS^3 is applied (Fig. 2b and c) but characteristically different from that of the VGE b_3. The presence of internal fragments from the b_3 ions of both G-γ-EVIG and γ-EVGIG suggests that the formation of a macrocycle structure for the b_3 of both analog peptides is both energetically and kinetically feasible. Nucleophilic attack by the N-terminus on the oxazolone carbonyl carbon for these peptides yields an 11-membered macrocycle rather than to the normal 9-membered ring of a b_3 macrocycle as shown in Fig. 3a and b. All of the internal fragment ions seen in these two spectra can be seen in the MS^3 spectrum of VGE, although the intensity of fragments such as the EV b_2 (m/z 229) and EV b_2-H_2O (m/z 211) are greatly reduced in intensity relative to the GE b_2. This pattern is opposite to that seen in the fragmentation behavior of protonated G-γ-EVIG and γ-EVGIG, wherein the EV fragments are significantly more intense than the GE fragment. This disparity in the spectra may be the result of 11-membered macrocycle formation by different pathways; the b_3 of VGEIG must isomerize through an anhydride structure before it can form an 11-membered cycle, whereas the γ-glutamic acid analogs presumably isomerizes to this structure after first forming an oxazolone, as has been shown by Paizs and co-workers in a study of YAGFL and analog peptides [40]. Thus, it is conceivable that internal energy differences may exist that could alter the ratios of b_3 macrocycle fragment ions. Fragmentation of VG-γ-EIG is not shown because QCID of the precursor did not yield any b_3 (see Supplementary Information, Fig. S2), which may further support that cyclization occurs via isomerization from an oxazolone structure; the standard oxazolone formation pathway would yield a 7-membered oxazolone-like b_3 structure in VG-γ-EIG, which may be kinetically unfavorable. Theoretically, b_3 anhydride formation is possible for VG-γ-EIG, however, the flexible carbon chain is integrated into the backbone rather than the side chain, which may kinetically constrain the extent to which nucleophilic attack can occur by this pathway.

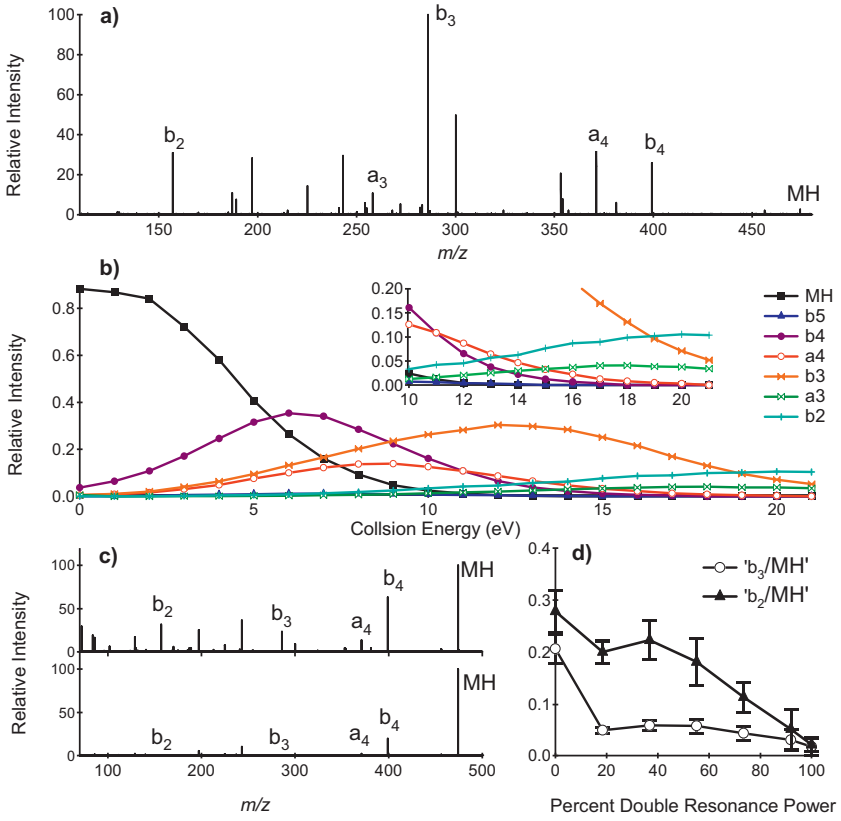

Fig. 1. (a) QCID MS/MS spectrum of protonated VGEIG at a collision energy of 12 eV. (b) Energy resolved mass spectra plots of protonated VGEIG by QCID. Dominant b_3 and b_2 ions are evidence for labile fragmentation C-terminal to glutamic acid and rapid fragmentation to b_2. (c) Double resonance of the b_3 during fragmentation (SORI) of the MH at the maximum applied double resonance energy. (d) The ratio of b_3 and b_2 relative to the $(M+H)^+$ as a function of the amplitude of the double resonance waveform.

3.2. Computational modeling of VGE b_3

Table 1 shows the five lowest energy b_3 ion conformations (1–5, wherein 1 is the lowest energy conformation, 2 is the second lowest energy structure and so on) of the anhydride, oxazolone, 9-membered macrocycle, and 11-membered macrocycle, all relative to the lowest energy conformation of the anhydride (anhydride 1). The lowest energy conformations of each b_3 structure are shown in Supplementary Information, Fig. S3. Although the anhydride structure is lowest in energy, the oxazolone is only 3.87 kcal/mol higher in energy. The relative energies of the lowest energy conformations of the two macrocycles are significantly different, with the 11-membered cycle being nearly 11 kcal/mol lower, which is consistent with apparent dominance of an 11-membered macrocycle

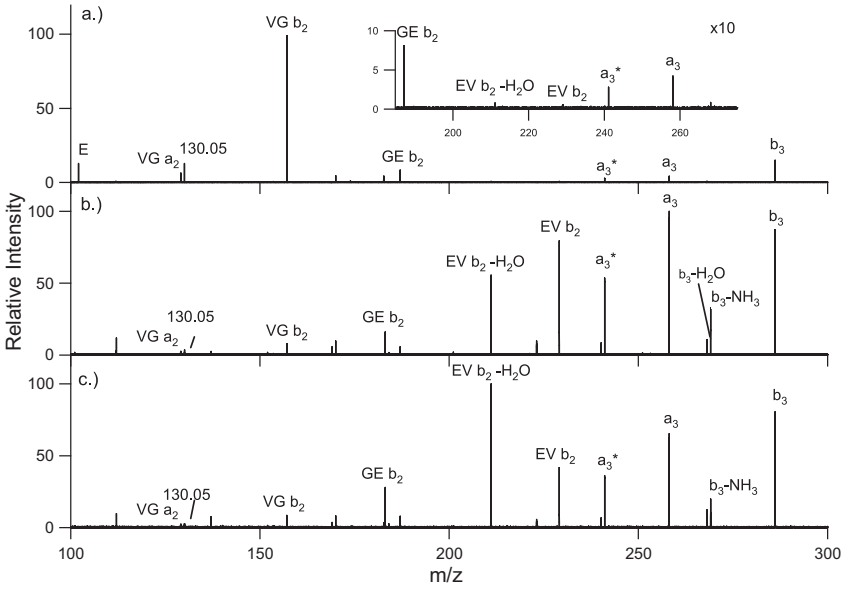

Fig. 2. MS^3 fragmentation spectra of the b_3 ion generated from (a) VGEIG, (b) G-γ-EVIG, and (c) γ-EVGIG. Inset shows a ten times magnification of (a) in the *m*/*z* range of 185–275.

Table 1
Five lowest energy conformations of each of the considered VGE b_3 structural isomers, relative to anhydride structure (a), in kcal/mol. Descriptions of significant bridging are shown in italics below the relative energy of each structure. Atoms are numbered by type (i.e., nitrogen) starting from the N-terminus and the atom listed first formally carries the charge.

Structure	Anhydride	Oxazolone	9-Membered macrocycle	11-Membered macrocycle
1	0.00	3.87	11.25	0.43
	N1–O3	*N1–O4*	*O3–O4*	*O2–O4*
2	2.82	4.46	17.58	1.38
	N1–O5, O1–N1	*N1–O4, O5–O1*	*O3, N3–O4*	*O3–O4*
3	2.87	4.58	18.37	3.07
	N1–O2	*N1–O4, O5–O2*	*O3, N3–O4*	*O3–O1*
4	4.66	4.90	19.15	4.80
	N1–O2, O3	*N1–O4, O5–N3*	*O2–O4*	*O1–O3, N1–O4*
5	4.88	5.24	19.65	6.84
	N1–O1	*N3–O5, N1–O4*	*O3–O5*	*O3–O4, O5–O2*

in the G-γ-EV and γ-EVG b_3 populations (see Fig. 2) relative to the absent 9-membered macrocycle population in the GEV and EVG b_3 ions (see Supplementary Information, Fig. S1). The experimental IRMPD action spectrum of the b_3 of VGEIG is shown in Fig. S4a; the computed IR spectra for the lowest energy conformations of an anhydride, oxazolone, extended macrocycle, and macrocycle are shown in Supplementary Information, Fig. S4b–f. The experimental spectrum shows a strong band at approximately 1700 cm^{-1} as well as weaker stretches in the range from 1100 to 1425 cm^{-1} and a very weak band at 1875 cm^{-1}. As both anhydride structures and the oxazolone show bands in these regions, it is not possible to definitively assign or eliminate either the anhydride or oxazolone contributions to the VGE b_3 IRMPD action spectrum. If present, the 11-membered macrocycle is of relatively low abundance, as the pattern of its bands only overlaps with the fringes of the major experimental bands.

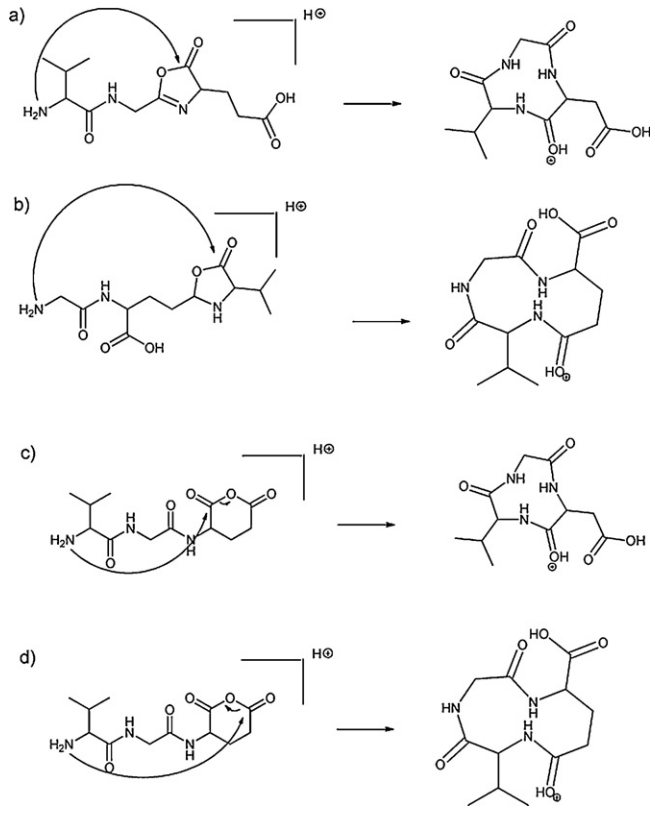

Fig. 3. Nucleophilic attack of the N-terminus on the oxazolone carbonyl carbon of the b_3 VGE oxazolone yields a 9-membered macrocycle in (a) and an 11-membered macrocycle when gamma-glutamic acid is substituted for alpha-glutamic acid, as shown in (b) for a G-γ-EV b_3 oxazolone structure. These same structures can be generated by N-terminal attack on the anhydride carbonyl carbons of a VGE b_3 anhydride structure, as shown in (c) and (d).

3.3. VGEIG methyl ester

O-methylation of the side chain and C-terminal carboxylic acid moieties was used to prevent nucleophilic attack by the side chain carboxylic acid on the glutamic acid amide carbon (amide #3). As shown in Fig. 4a, transfer of the carboxylic acid proton is assumed to be necessary to form an anhydride structure and substitution of a methyl for this proton renders this pathway inaccessible. Fig. 5 shows the MS^3 spectra of a b_3 of VGEIG (a) and VGE(OMe)IG(OMe) (b). The two spectra demonstrate little if any similarities in fragmentation behavior, but the most striking features of the spectrum of the VGE methyl ester are the near complete absence of a b_2 ion and the increased intensity of the a_3 and a_3^* (a_3-NH_3) pair. From this, it can be concluded that nearly all of the b_2 formed in the unmodified VGEIG system originates from a b_3 anhydride precursor. This is particularly useful for the study of secondary cleavage N-terminal to glutamic acid as it allows an exclusive focus on the anhydride in a mechanistic approach to probing the formation of the b_2 species. Also absent in the fragmentation spectrum of the O-methylated b_3 are the GE (m/z 187) and m/z 130.05 ions, suggesting that while O-methylation of glutamic acid does not prevent b_3 formation, it does prevent formation of b_3 anhydride and extended macrocycle. Absence of these ions is evidence for the pathway shown in Fig. 4, wherein the internal fragment GE is formed from the extended macrocycle, a structure that can only form via anhydride formation and subsequent isomerization to the macrocycle. A feature of note is that the b_2 ion appears to be generated almost exclusively from the anhydride b_3 structure; the methyl ester b_3 structure, presumably an oxazolone, forms a negligible amount of the b_2 ion, even at very high collision energies (Supplementary Information, Fig. S5).

Fig. 4 shows a proposed pathway that describes the formation of the b_3 anhydride as well as b_2, GE b_2, and the m/z 130.05 ions from this anhydride b_3 structure. It is expected that the presence of the amino terminus and oxazolone ring nitrogen in the b_2 ion and single primary amine in the anhydride ring fragment would yield more charge retention on the b_2 fragment; this is observed as the ratio of ion intensities between the b_2 and amino substituted anhydride ring fragment is approximately 10:1 (see Fig. 5). Isomerization of the VGE extended macrocycle to a GEV b_3 oxazolone and subsequent degradation to either an anhydride or oxazolone analog GE b_2 explains the presence of GE in the MS^3 fragmentation of the VGEIG b_3.

3.4. IRMPD action spectroscopy: b_2 structures

IRMPD action spectroscopy was performed on the b_2 ion generated from protonated VGEIG. Fig. 6a–c shows the experimental

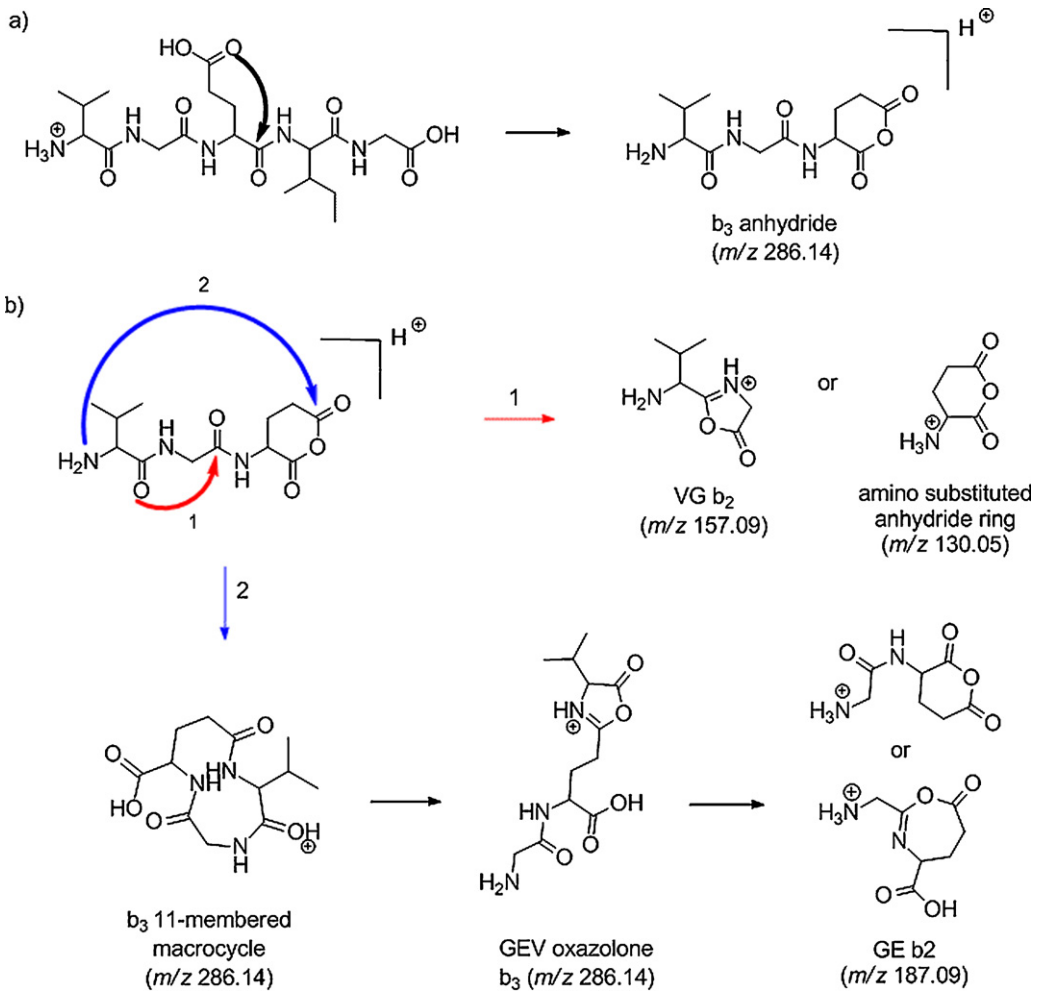

Fig. 4. Proposed pathway for (a) the formation of VGE b_3 anhydride, (b) anhydride degradation to b_2 or m/z 130.05 and anhydride isomerization to an extended macrocycle and subsequent fragmentation to a GE b_2.

spectra generated for all fragment ions, only the a_2 ion, and only the a_1 (valine immonium fragment) ion, respectively. When all fragments are included in the experimental fragmentation efficiency spectrum, three separate bands at 1915, 1935 and 1955 cm^{-1} are observed (see Fig. 6a, black trace). As this region is known to correspond to conjugated and ring carbonyls, the spectrum suggests the presence three chemically distinct carbonyls, most likely present in one or two unique structures. Fig. 6d–f shows the computed IR spectra for the ring nitrogen protonation of the oxazolone structure and two conformations of the N-terminally protonated oxazolone structure. In Fig. 6d, the computed IR spectrum for the ring protonated oxazolone is shown and can be seen to be an excellent match with the experimental spectrum summed only over the a_1 ion. Although many of the low intensity bands below 1400 cm^{-1} do not appear in the experimental spectrum, all of the major bands in the spectrum are in good agreement with the experimental spectrum. The only other disparity between the experimental and computed spectra is the reduced intensity of the experimental band at 1955 cm^{-1} and increased intensity of the experimental band at 1425 cm^{-1} relative to the computed spectrum but this can at least partially be attributed to inefficient compensation for the decreasing laser power in the wavenumber range of 1800–2000 cm^{-1}.

Although the carbonyl stretches at 1915 and 1935 cm^{-1} are missing in Fig. 6c (a_1 ion), they are present in the action spectrum summed over the a_2. This suggests that a single structure generates the a_1 ion, leaving a second and possibly a third structure that appear to be particularly prone to forming a_2. The ring carbonyl band in Fig. 6e, corresponding to an N-terminally protonated oxazolone weakly bridged to the ring nitrogen, is centered at 1925 cm^{-1} and is shifted nearly 10 cm^{-1} from the center band in the triplet of experimental ring carbonyl stretches. The band at 1650 cm^{-1}, corresponding to a symmetric ammonia stretching mode, is also shifted from a band in the experimental a_2 only spectrum (Fig. 6c). Therefore, it is not possible to confidently assign these bands to this conformation, although this structure is energetically fairly stable and may be present in low to mid abundance. It is additionally possible that an anharmonic well for the minimized structure has caused the computed bands to be somewhat shifted from their true values. In Fig. 6f, the IR spectrum for the N-terminally protonated oxazolone with a ring oxygen bridge is shown. A ring carbonyl stretching mode appears at 1915 cm^{-1}, which is in good agreement with the experimental band at 1914 cm^{-1}. However, as is the case with the N-terminally protonated, N-bridged conformer, a band at 1700 cm^{-1} cannot be accounted for by comparison to the experimental spectrum. Thus, this conformation also cannot be confidently assigned, although the absence of this band in the experimental spectrum could also be the result of a shift due to an anharmonic energy well. In spite of these ambiguities, IRMPD action spectroscopy confirms the presence of the oxazolone ring N-protonated form, and is presumably a dominant structure for b_2.

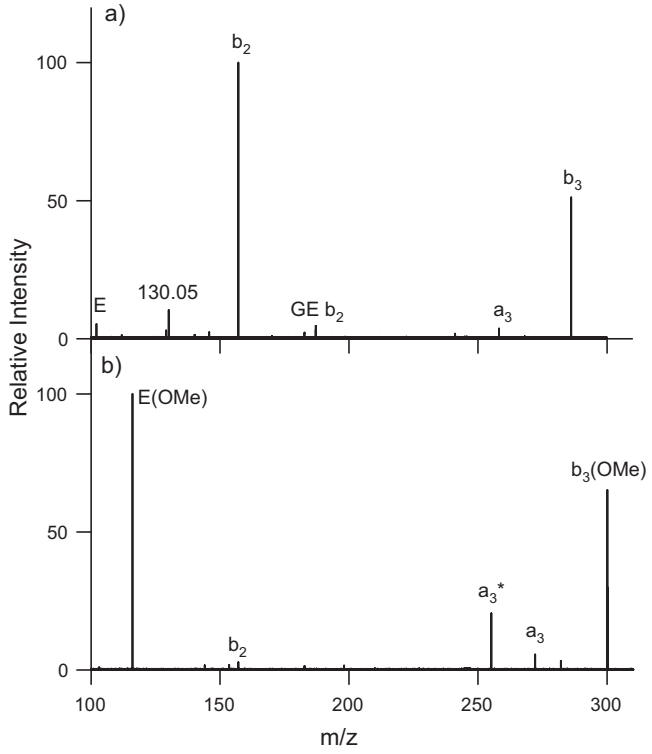

Fig. 5. MS^3 spectra of the b_3 generated from protonated (a) VGEIG and (b) VGE(OMe)IG(OMe).

3.5. QCID-HDX-SORI – b_2 formation

In order to probe the fragmentation pathway(s) for the formation of b_2 from b_3, MS^3, HDX, and QCID-HDX-SORI experiments were performed on a series of VXEIG analogs (wherein X was L-alanine (A_L), D-alanine (A_D), and 2-aminoisobutyric acid (Aib)). A hydrogen–deuterium exchange (HDX) spectrum of the b_3 of VGEIG is shown in Fig. 7a-1 (obtained following a 20 s exchange at 1×10^{-7} mbar CD_3OD pressure). A single Gaussian distribution with a maximum of five exchanges is consistent with an anhydride structure, which is able to exchange five protons. Similarly, an HDX spectrum of the VGEIG b_2 obtained with the same experimental conditions is shown in Fig. 7-2a; a maximum of three exchanges is consistent with an oxazolone structure. The D_5 ion of the b_3 exchange distribution has been fragmented by SORI (QCID-HDX-SORI) and the subsequent isotope distribution of the b_2 is shown in Fig. 7-3a. The presence of a D_4 and D_5 peak in the b_2 distribution implicates the involvement of a hydrogen from an aliphatic carbon during the fragmentation of the b_3. The spectra in Fig. 7b–d were obtained by the same HDX and QCID-HDX-SORI experiments that were performed on VXEIG analogs, where X is A_L, A_D, and (Aib), respectively. A maximum of five exchanges is observed for each of the b_3 analogs and three exchanges is observed for each of the b_2 analogs. SORI fragmentation of the D_5 population in the b_3 distribution of each of these analogs is evidence for alpha proton involvement during the fragmentation of the b_3 ion. The addition of a single methyl (VA_LEIG and VA_DEIG) eliminates the D_5 population from the b_2 isotope distribution and reduces the intensity of the D_4 by approximately half (Fig. 7-3b and c). Replacement of the remaining alpha proton with another methyl (V(Aib)EIG, Fig. 7-3d) results in the complete elimination of the D_4 and D_5 peaks, suggesting the source of the unlabeled protons that are involved in the fragmentation of the b_3 is exclusively the alpha (carbon) protons of the second residue. The strong similarity in the isotope patterns in Fig. 7-3b and c interestingly suggest that the involvement of the alpha protons is not stereo-specific. Multiple pathways are needed to describe the formation of the b_2 from the b_3 based on QCID-HDX-SORI experiments, in which alpha protons are non-steroselectively involved in roughly half of the fragmentation processes.

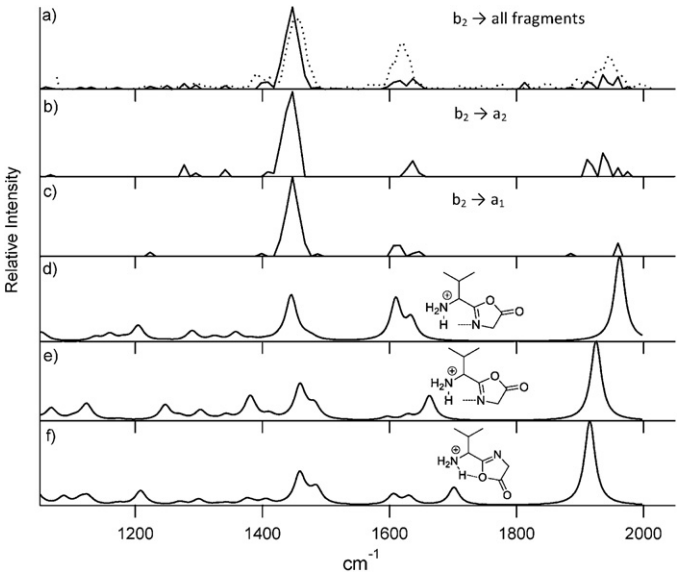

Fig. 6. Experimental and calculated IRMPD action (dissociation) spectra of the b_2 ion of VGEIG. The fragmentation efficiency of different fragments is plotted against frequency. In (a) all fragments are combined with different technical replicates run months apart shown in solid and hashed traces, respectively, with b and c taken from replicate 1. In (b) only the a_2 is included while in (c) only the valine immonium ion (a_1) is included. In (d–f), the calculated spectra for the lowest energy conformations of an oxazolone are shown. Spectrum (d) corresponds to protonation on the oxazolone ring nitrogen, (e) to the N-terminus and bridged to the ring nitrogen, and (f) to the N-terminus and bridged to the ring oxygen.

Fig. 8 shows the QCID-SORI MS^3 spectra of the b_3 of VGEIG and VG(2,2-d_2)EIG, in which the alpha carbon of the glycine residue has been labeled with two deuteriums. The isotope distribution of the b_2 ion is further evidence for alpha hydrogen (proton) involvement during the formation of b_2 from b_3, as the doubly deuterated b_3 forms a distribution (D_0, D_1, and D_2) of b_2 ions inversely analogous to the distribution seen in Fig. 7-3a. The m/z 158 peak in Fig. 8b represents the singly deuterated b_2, wherein an alpha deuterium has been replaced with an unlabeled hydrogen (proton). For simplicity, this will be referred to as scrambling. Theoretically, an alpha proton scrambling event could occur at several times during the formation of the b_2, however, only during a post-dissociation event can both alpha protons scramble. It has been well demonstrated by Morton and co-workers that ion–molecule complexes exist sufficiently long in the gas phase for ion–molecule reactions to occur [41,42]. The observed alpha proton scrambling is thus a secondary pathway occurring during the lifetime of the ion–molecule complex formed between the VG b_2 and the neutral amino-substituted anhydride ring. In the inset of Fig. 8b, an isotope distribution of the charged amino-substituted anhydride ring (m/z 130.05) is evidence for its involvement in the formation of the "scrambled" b_2 population. In addition, by combining the intensities of the m/z 131 and 132 (1st and 2nd scrambling peaks of the amino-substituted anhydride ring), scrambling can be estimated to occur in roughly 55% of the charged amino-substituted anhydride ring population (m/z 130.05). In contrast, scrambling occurs in roughly 45% of the b_2 population. This disparity in scrambling propensity is likely the result of a two-step scrambling process, in which removal of the alpha proton yields a charged amino-substituted anhydride ring (m/z 130.05) and neutral "b_2"

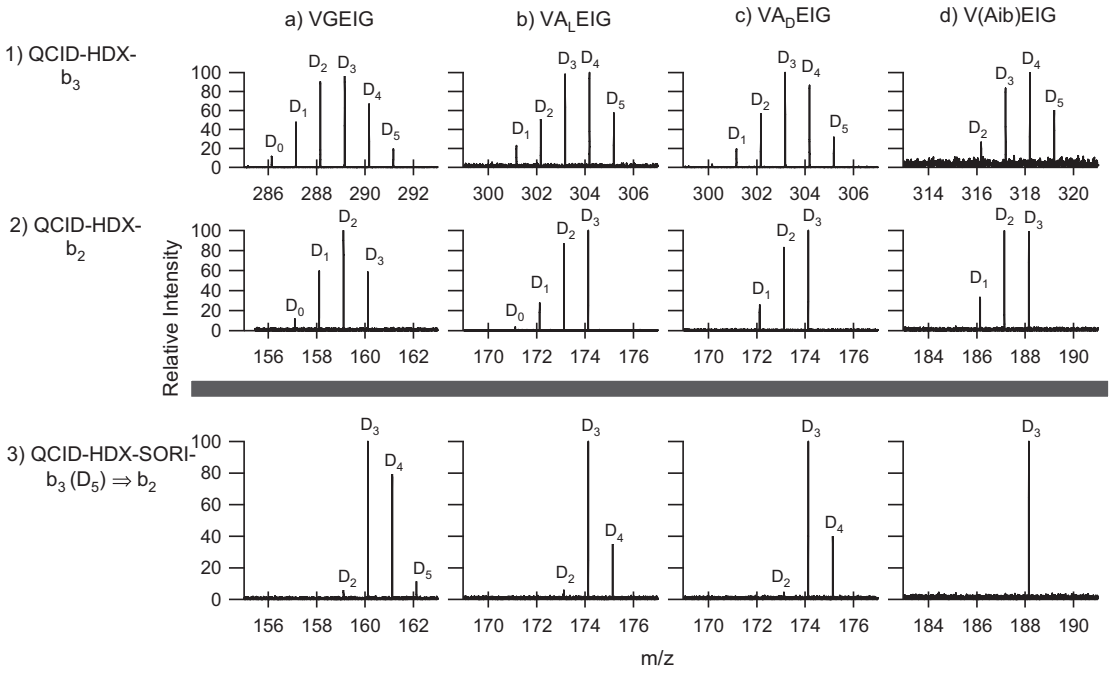

Fig. 7. QCID-HDX using a 20 s pulse of CD_3OD at 1×10^{-7} mbar of the b_3 and b_2 as well as QCID-HDX-SORI of the D_5 of the b_3 of (a) VGEIG, (b) VA_LEIG, (c) VA_bEIG, and (d) V(Aib)EIG.

in the first step, and charge transfer back to the oxazolone in the second step regenerates the b_2 ion. Dissociation of the complex before the second charge transfer would yield the charged and scrambled amino-substituted anhydride ring, giving the appearance that the anhydride has a larger scrambled population for this ion relative to the b_2.

3.6. Transition state modeling

In a study of the formation of a_3^* (a_3-NH_3) ions, Paizs and co-workers reported alpha proton scrambling (see Supplementary Information, Fig. S6). However, by the mechanism they proposed, the transfer of an alpha proton occurs simultaneously with the back transfer of an ammonia proton, resulting in the formation of a b_2 enol ion [43]. This pathway is inconsistent with our present findings of the disparate extents of scrambling in the b_2 and charged amino-substituted anhydride ring. The b_2 enol structure is also inconsistent with our experimental IRMPD action spectroscopy measurements (see Supplementary Information, Fig. S7). Moreover, near identical MS^3 and HDX of the D_0–D_2 of the VG(2,2-d2)EIG b_2 suggest that the scrambled and unscrambled b_2 ions have the same structure (see Supplementary Information, Fig. S8). In order

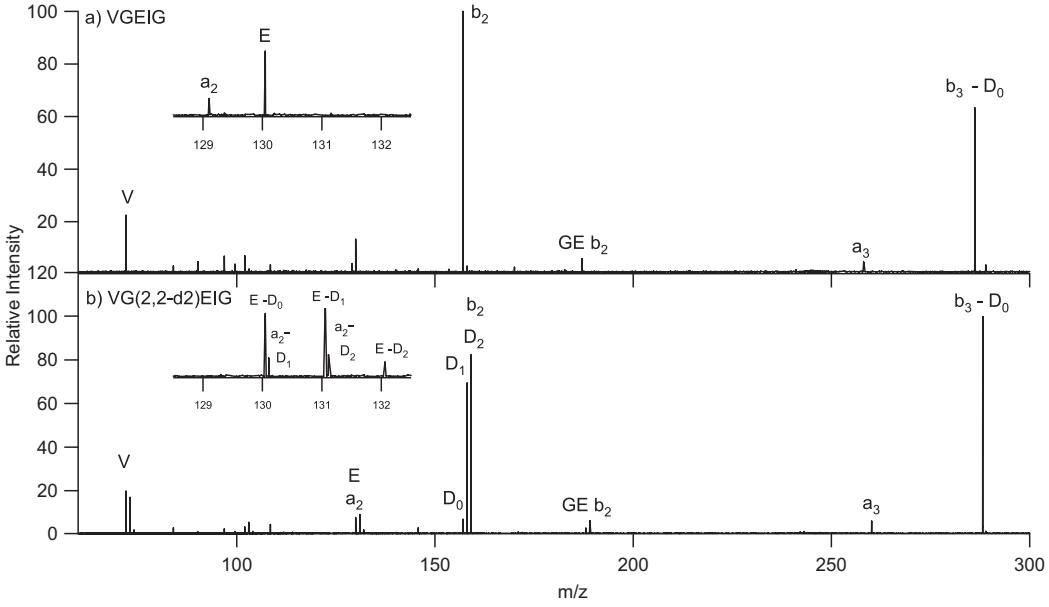

Fig. 8. QCID-SORI of b_3-D_n of (a) VGEIG and (b) VG(2,2-d2)EIG. The "triplet" (D_0, D_1 and D_2) of b_2 ions is evidence for a second pathway for the formation of b_2 from b_3 wherein the alpha proton is lost with the neutral loss fragment. In the deuterated analog, this yields a peak at m/z 158. Insets (a) and (b) show a magnification of the region between m/z 128 and 133, which contains both the a_2 ion as well as the m/z 130.05 fragment.

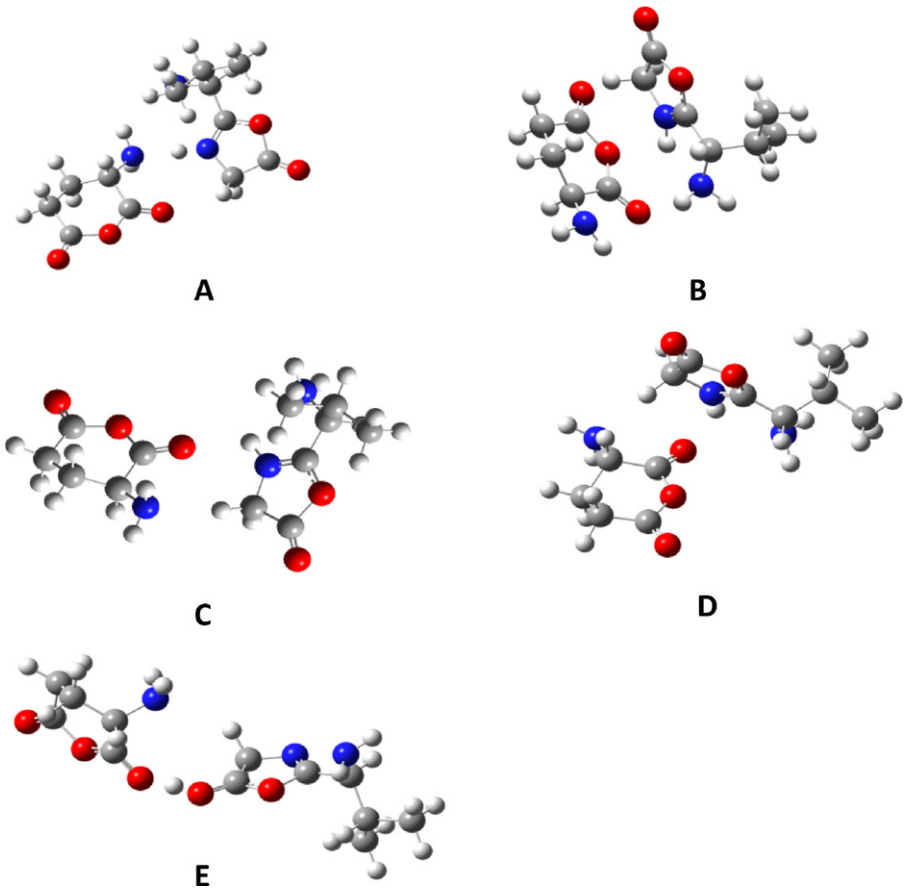

Fig. 9. Lowest energy configurations in which a basic site of the anhydride ring is within 3 Å of an alpha proton.

to elucidate the potential energy surface (PES) of the multi-step scrambling pathways enumerated above, all stable configurations of an ion–molecule complex were determined using a Monte Carlo conformational search. Of the 26 stable conformations discovered, 5 were in an orientation in which a basic site of the amino-substituted anhydride ring was within 3 Å of an alpha proton. These candidate structures are shown in Fig. 9. In configuration A, the amino group of the anhydride ring is hydrogen bonded to the oxazolone ring nitrogen, allowing the proximal anhydride carbonyl to bridge to the alpha carbon. Both anhydride carbonyls are bridged in B, one to the N-terminus and one to an alpha hydrogen. In conformation C, the anhydride is flipped relative to A, with the anhydride proximal carbonyl engaged in hydrogen bonding with the oxazolone ring nitrogen and the amino group bridging to the alpha hydrogen. In conformation D, the orientation of the anhydride ring is very similar to C, but the proximal anhydride carbonyl

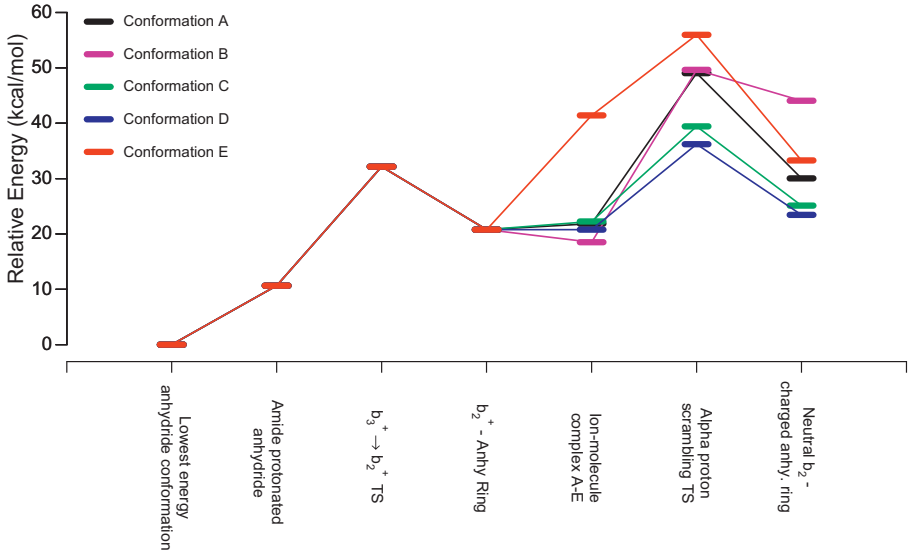

Fig. 10. Energy landscape of the fragmentation of the VGE b_3^+ anhydride.

is tethered by electrostatic attractions to the ring nitrogen rather than hydrogen-bonds. Finally, in conformation E, a hydrogen bond between the oxazolone carbonyl and the anhydride carbonyl stabilizes the complex and allows for a weak bridging between the amino group of the anhydride ring and alpha proton. (Note that structures A–E are all local minima on the PES.)

Transition states (TS) and the relaxed neutral oxazolone-charged anhydride ring conformations were computed for all five starting conformations. The resulting energy landscape for each pathway is shown in Fig. 10. For comparison, the TS energy for the formation of the b_2 is also shown. Of the five examined conformations, only in C and D is the energy of the TS is less than 10 kcal/mol higher in energy than the TS calculated for the formation of the b_2. Following deprotonation of the alpha proton, both conformations form a neutral ring that is hydrogen bonded by the charging proton to the amino substituted anhydride ring, both of which are less than 5 kcal/mol higher in energy than the charged b_2 following its formation. The relatively low energy change, both for the transition state and the products is consistent with the experimental alpha scrambling behavior, wherein scrambling occurs even at the lowest collision energies applied (and increases with increasing collision energy, see Supplementary Information, Fig. S9). The relative similarity in the two configurations, that is, hydrogen bonding vs. electrostatic attraction as the stabilizing force, makes it likely that they both are routes via which alpha hydrogen scrambling occurs. However, as pathway D is lower in energy by 3 kcal/mol at the transition state and 1.5 kcal/mol at the products, it is thermodynamically and kinetically the better candidate.

4. Conclusions

Enhanced cleavage at the amide bond located C-terminal to glutamic acid in the protonated pentapeptide VGEIG has been demonstrated here to be the direct result of formation of a stable b_3 anhydride structure. This is the dominant b_3 structure, which is able to directly fragment to a standard b_2 oxazolone structure. As the formation of b_2 ions from b_3 ions has until now been proposed via a high energy a_3 intermediate, the direct "anhydride" pathway may make b_2 formation significantly more facile and result in a more abundant b_2 population in the case of glutamic acid containing b_3 ions. In addition, we see evidence for alpha hydrogen scrambling during the formation of the b_2 and propose that this occurs by a multi-step pathway in which the b_2 and neutral loss fragment form a stable ion–molecule complex. Extraction of the alpha proton by the amino group of the anhydride ring is facilitated by stabilizing electrostatic interactions between the anhydride carbonyl and the oxazolone ring nitrogen; deprotonation generates a neutral b_2 ring structure as an intermediate to a second step in which the b_2 oxazolone can be regenerated. The low energies of the transition state and ion–molecule complexes of this mechanism permit alpha proton scrambling to occur at very low collision energies, consistent with experimental evidence. QCID-HDX-SORI is emerging as an extremely useful diagnostic tool for the elucidation fragment ion structures and reaction mechanisms, and interpretation of the isotope distributions of product ions is critical in order to correctly assign structures to HDX distributions. Thus, understanding alpha proton scrambling is necessary in order to maximize the information that can be obtained from this technique.

The present work additionally demonstrates the necessity of using multiple different experimental techniques (such as MS/MS, MS^3, double resonance, HDX, and IRMPD action spectroscopy) as well as theoretical (quantum chemical) calculations to elucidate the details of gas phase fragmentation mechanisms and ion structures even in a relatively small (penta)peptide.

Acknowledgments

Professor Eugene Nikolaev is acknowledged for his many contributions to ion cyclotron resonance mass spectrometry, in particular his efforts to elucidate the dynamic trajectories of ions within an ICR and thereby improving the resolution of the spectrometer. This research is supported by the National Institute of Health, under grant R01 051387. The CLIO institute in Orsay, France is thanked for access to their free electron laser and ion trap. The CLIO staff, Ashley Gucinski, and Julia Chamot-Rooke are thanked for their help in acquiring the IRMPD spectra shown here. The University of Arizona mass spectrometry facility is additionally thanked for providing access to the FT-ICR purchased with NIHEI grant 1S10RR023029-01.

Appendix A. Supplementary data

Supplementary data associated with this article can be found, in the online version, at http://dx.doi.org/10.1016/j.ijms.2012.08.012.

References

[1] P. Roepstorff, J. Fohlman, Biological Mass Spectrometry 11 (1984) 601.
[2] K. Biemann, Biomedical and Environmental Mass Spectrometry 16 (1988) 99.
[3] D. Perkins, D. Pappin, D. Creasy, J. Cottrell, Electrophoresis 20 (1999) 3551.
[4] J.K. Eng, A.L. McCormack, J.R. Yates Iii, Journal of the American Society for Mass Spectrometry 5 (1994) 976.
[5] L. Geer, S. Markey, J. Kowalak, L. Wagner, M. Xu, D. Maynard, X. Yang, W. Shi, S. Bryant, Journal of Proteome Research 3 (2004) 958.
[6] S. Molesworth, S. Osburn, M. Van Stipdonk, Journal of the American Society of Mass Spectrometry 21 (6) (2010) 1028.
[7] A.L. McCormack, A. Somogyi, A.R. Dongre, V.H. Wysocki, Analytical Chemistry 65 (1993) 2859.
[8] S.G. Summerfield, A. Whiting, S.J. Gaskell, International Journal of Mass Spectrometry and Ion Processes 162 (1997) 149.
[9] A.R. Dongré, J.L. Jones, Á. Somogyi, V.H. Wysocki, Journal of the American Chemical Society 118 (1996) 8365.
[10] S.G. Summerfield, S.J. Gaskell, International Journal of Mass Spectrometry and Ion Processes 165–166 (1997) 509.
[11] A. Goloborod'ko, C. Mayerhofer, A. Zubarev, I. Tarasova, A. Gorshkov, R. Zubarev, M. Gorshkov, Journal of Analytical Chemistry 65 (2010) 1462.
[12] W. Li, L. Ji, J. Goya, G. Tan, V.H. Wysocki, Journal of Proteome Research 10 (2011) 1593.
[13] A. Somogyi, Journal of the American Society for Mass Spectrometry 19 (2008) 1771.
[14] J. Lemaire, P. Boissel, M. Heninger, G. Mauclaire, G. Bellec, H. Mestdagh, A. Simon, S.L. Caer, J.M. Ortega, F. Glotin, P. Maitre, Physical Review Letters 89 (2002) 273002.
[15] B.C. Bohrer, S.I. Merenbloom, S.L. Koeniger, A.E. Hilderbrand, D.E. Clemmer, Annual Review of Analytical Chemistry 1 (2008) 293.
[16] V.H. Wysocki, G. Tsaprailis, L.L. Smith, L.A. Breci, Journal of Mass Spectrometry 35 (2000) 1399.
[17] B. Paizs, S. Suhai, Mass Spectrometry Reviews 24 (4) (2005) 508.
[18] Z. Zhang, Analytical Chemistry 76 (2004) 3908.
[19] K. Hermann, V. Wysocki, Journal of the American Society of Mass Spectrometry 16 (7) (2005) 1067.
[20] C. Gu, G. Tsaprailis, L. Breci, V.H. Wysocki, Analytical Chemistry 72 (23) (2000) 5804.
[21] J. Qin, B.T. Chait, Journal of the American Chemical Society 117 (1995) 5411.
[22] G. Tsaprailis, H. Nair, Á. Somogyi, V.H. Wysocki, W. Zhong, J.H. Futrell, S.G. Summerfield, S.J. Gaskell, Journal of the American Chemical Society 121 (1999) 5142.
[23] S.-W. Lee, H.S. Kim, J.L. Beauchamp, Journal of the American Chemical Society 120 (1998) 3188.
[24] R.A. Jockusch, P.D. Schnier, W.D. Price, E.F. Strittmatter, P.A. Demirev, E.R. Williams, Analytical Chemistry 69 (1997) 1119.
[25] R. Bakhtiar, Q. Wu, S.A. Hofstadler, R.D. Smith, Biological Mass Spectrometry 23 (1994) 707.
[26] A.G. Harrison, Journal of Mass Spectrometry 128 (32) (2003) 174.
[27] L. Men, Y. Wang, Rapid Communications in Mass Spectrometry 19 (2005) 23.
[28] G. Tsaprailis, Á. Somogyi, E.N. Nikolaev, V.H. Wysocki, International Journal of Mass Spectrometry 195–196 (2000) 467.
[29] J.D. Baldesch-Wieler, J.L. Beauchamp, P.M. Liewellyn, Varian Associates, 1968, p. 16, Patent no. FR 1531956.
[30] A.G. Myers, J.L. Gleason, T. Yoon, D.W. Kung, Journal of the American Chemical Society 119 (1997) 656.
[31] E. Atherton, R.C. Sheppard (Eds.), Solid-Phase Peptide Synthesis: A Practical Approach, Oxford University Press, Oxford, 1989.
[32] B. Lucas, G. Grégoire, J. Lemaire, P. Maître, F. Glotin, J.P. Schermann, C. Desfrançois, International Journal of Mass Spectrometry 243 (2005) 105.
[33] L. Schrödinger, Macromodel, version 9.9, Schrödinger, Inc., New York, NY, 2011.

[34] A.G. Harrison, A.B. Young, Journal of the American Society for Mass Spectrometry 15 (2004) 1810.
[35] J.M. Allen, A.H. Racine, A.M. Berman, J.S. Johnson, B.J. Bythell, B. Paizs, G.L. Glish, Journal of the American Society for Mass Spectrometry 19 (2008) 1764.
[36] T. Yalcin, C. Khouw, I.G. Csizmadia, M.R. Peterson, A.G. Harrison, Journal of the American Society for Mass Spectrometry 6 (1995) 1165.
[37] N.C. Polfer, J. Oomens, S. Suhai, B. Paizs, Journal of the American Chemical Society 127 (2005) 17154.
[38] J. Yagüe, A. Paradela, M. Ramos, S. Ogueta, A. Marina, F. Barahona, J.A. López de Castro, J. Vázquez, Analytical Chemistry 75 (2003) 1524.
[39] X. Chen, J.D. Steill, J. Oomens, N.C. Polfer, Journal of the American Society for Mass Spectrometry 21 (2010) 1313.
[40] A.G. Harrison, A.B. Young, C. Bleiholder, S. Suhai, B. Paizs, Journal of the American Chemical Society 128 (2006) 10364.
[41] T.H. Morton, Organic Mass Spectrometry 27 (1992) 353.
[42] D.J. McAdoo, T.H. Morton, Accounts of Chemical Research 26 (1993) 295.
[43] T. Cooper, E. Talaty, J. Grove, M. Van Stipdonk, S. Suhai, B. Paizs, Journal of the American Society for Mass Spectrometry 17 (2006) 1654.